Protein Adsorption in Charged Agarose Gels Studied by Light Microscopy

Emily B. Schirmer and Giorgio Carta
Dept. of Chemical Engineering, University of Virginia, 102 Engineers' Way, Charlottesville, VA 22904

DOI 10.1002/aic.11191
Published online May 1, 2007 in Wiley InterScience (www.interscience.wiley.com).

Both a new method for measuring protein ion exchange kinetics and new data for the adsorption of three different proteins in anionic agarose gels are described. The gels were prepared as spherical particles to determine chemical and structural properties and the macroscopic protein adsorption behavior, and as thin slabs supported in a microfluidics chip to observe transient concentration profiles with a light microscope. The combination of these approaches provides deeper insight in the nature of protein transport mechanisms than previously possible. The adsorption of cytochrome c, myoglobin, and hemoglobin was studied macroscopically and microscopically. Although all proteins exhibited similarly favorable adsorption isotherms, adsorption kinetics, and concentration profiles were quantitatively and qualitatively different. Cytochrome c was adsorbed very quickly and resulted in diffuse concentration profiles, while myoglobin adsorbed much more slowly and resulted in sharp fronts. Hemoglobin exhibited lower rates with diffuse profiles at higher pH and sharp fronts at lower pH. In general, the shape of the profiles appeared to be correlated with the binding strength. Reversibly bound proteins yielded diffuse profiles, while irreversibly bound proteins exhibited sharp advancing fronts, indicating that protein–surface interactions play a major role in the nature of the transport mechanism. © 2007 American Institute of Chemical Engineers
AIChE J, 53: 1472–1482, 2007
Keywords: protein adsorption, ion exchange, mass transfer, visualization, modeling

Introduction

Intraparticle diffusion is often rate controlling in protein ion exchange chromatography. Thus, it is desirable to understand the mass transfer mechanism to predict chromatographic performance or design optimal stationary phases.[1,2]

In general, intraparticle mass transfer in adsorption systems can be thought of as the result of two distinct mechanisms—pore diffusion and diffusion in the adsorbed phase.[3,4] In pore diffusion, the adsorbed solute diffuses in liquid-filled pores whose size is sufficiently large to allow transport to occur unaffected by interactions with the adsorbent surface. On the other hand, transport in the adsorbed phase occurs while the adsorbate molecules continuously interact with the adsorbent surface. The latter can occur, for example, in a charged network structure or within the electrical double-layer of a charged surface. These mechanisms are widely different; however, their differences are not evident in macroscopic uptake data. Figure 1 shows, as an example, simulated results for adsorption with a highly favorable adsorption isotherm for pore diffusion and for diffusion in the adsorbed phase. As seen in Figure 1a, the macroscopically observable adsorption kinetics given by the average adsorbed concentration as a function of time is insensitive to the mass transfer mechanism. Indeed, this trend has also been seen experimentally in protein adsorption studies where pore and homogeneous diffusion models have both been used to fit batch uptake data with equal accuracy.[5–7] On the other hand, as seen in Figure 1b, the two mechanisms can be readily distinguished at the microscopic level since sharp fronts are predicted for

Correspondence concerning this article should be addressed to Giorgio Carta at gc@virginia.edu.

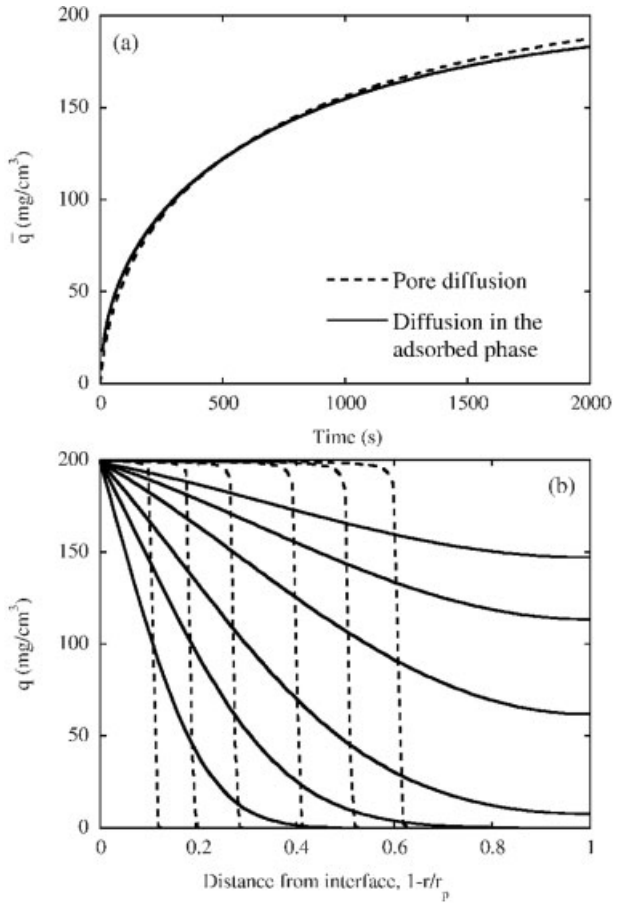

Figure 1. Simulated uptake curves (a) and adsorbed concentration profiles (b) for batch adsorption in 90 μm spherical particles with a favorable isotherm using pore and adsorbed phase diffusion models.

The isotherm was $q_3 = 800C/(1 + 80C)$ for both models with $C_0 = 2$ mg/cm^3. The diffusivities were $D_e = 1.8 \times 10^{-7}$ cm^2/s for the pore diffusion model and $D_s = 2 \times 10^{-9}$ cm^2/s for the adsorbed phase diffusion model. Profiles are shown at 100, 250, 500, 1000, 1500, and 2000 s.

pore diffusion while diffuse profiles are predicted for transport in the adsorbed phase.

Two methods have been used to observe intraparticle diffusion of proteins in ion exchange matrices; confocal microscopy of whole particles and light microscopy of slab-shaped matrices. Confocal laser scanning microscopy was introduced by Ljünglof and Hjorth[8] and has been used by several authors to observe protein concentration profiles in ion exchangers.[9–15] The technique detects the light emitted by a fluorescent molecule along thin optical sections of a clear or semitransparent particle. When used in protein adsorption studies, a trace amount of the protein is fluorescently labeled and used to determine the total protein concentration profile by assuming that the ratio of labeled and native protein in the adsorbent is the same as in solution. Unfortunately, however, as shown recently by Teske et al.,[16–17] fluorescent labeling can alter the adsorption properties of the protein on ion exchangers and result in fluorescence intensity profiles that do not represent the true protein concentration. The method also requires deconvolution of the signal, which is affected by fluorescence attenuation effects.[10,12,16,18]

Optical microscopy with chromophoric proteins adsorbing in a slab-shaped matrix has also been used to image protein concentration profiles.[19–21] The method has been applied to charged polyacrylamide gels synthesized in the lumen of a square-section quartz capillary and exposed to a protein solution by observing microscopically the evolution of the color intensity in the gel as a function of time and distance from the exposed interface. The rectilinear, semi-infinite slab geometry provides for simple data acquisition and analysis, but the method has been limited to matrices that can be synthesized in one step, such as charged polyacrylamide gels. Other ion exchangers, such as those based on agarose require multiple steps where a base matrix is first formed followed by various functionalization steps. Synthesizing such materials within a capillary could also be possible but it would be cumbersome and lengthy since long times are needed to allow the reactants to diffuse in the matrix at each step in the synthesis process. Thus, as an alternative, we have developed a microfluidics-based device that allows the preparation of thin, slab-shaped ion-exchangers by first casting a support matrix and then functionalizing it. After functionalization, the slab matrix is encased in a flow-cell, allowing reproducible contact with a protein solution at controlled flow rates. Concentration profiles in the slab are obtained by imaging with a microscope using chromophoric proteins.

In this article we provide both a description of the method and new data for the adsorption and transport of three different proteins (cytochrome c, myoglobin, and hemoglobin) in a negatively charged agarose gel obtained by functionalizing a neutral agarose matrix with sulfopropyl groups. Key physical properties of the gel are obtained by producing the same material in bead form and determining charge density, apparent pore size, and protein adsorption equilibrium isotherms and rates. Microscopic experiments reveal noticeably different concentration profiles in the gel for different proteins and for the same protein under different adsorption conditions, suggesting that different transport mechanisms are dominant in each case. A preliminary quantitative analysis of the results is performed using an effective pore diffusion model. The model parameters are then used to compare the rates of adsorption under different conditions and to reconcile macroscopic measurements of adsorption rates with the evolution of concentration profiles in the ion exchange matrix.

Materials and Methods

Materials

High gel strength agarose (gel temperature 36–42°C) was obtained from USB Corporation (Cleveland, OH). Agarose is comprised of repeating units of β-D galactose and 3,6-anhydro-α-L galactose linked together by ether bonds.[2] A macroporous structure comprised of α-helices held together by physical crosslinks forms upon cooling a hot aqueous agarose solution.[22] The gel can then be chemically crosslinked to increase mechanical strength and functionalized to introduce ionic groups.

Chemicals used to functionalize the agarose matrix were epichlorohydrin (EPC), allyl glycidyl ether (AGE), sodium hydroxide, sodium borohydrate, sodium sulfate, and sodium metabisulfite and were from Sigma (St. Louis, MO) and Fisher Scientific (Fair Lawn, NJ). Sodium phosphate, sodium acetate, and sodium chloride used in buffer preparations were from Fisher Scientific (Fair Lawn, NJ). Borofloat® glass spin-coated with chrome and photoresist was obtained from Nanofilms (West Lake, CA) and used to prepare the microfluidics chips using standard photolithographic techniques and wet chemical etching.[23] The photo mask was printed at 1200 dpi by EM Communications (Charlottesville, VA).

Dextran standards (T fractions) with 5, 10, 25, 40, 70, and 500 kDa molecular masses used in inverse size exclusion chromatography (iSEC) experiments were from GE Healthcare (Piscataway, NJ). Blue dextran and glucose used to determine the extraparticle porosity and total mobile phase volume, respectively, were from Sigma Chemical (St. Louis, MO).

Cytochrome c (bovine, $M_r = 12.5$ kDa, pI 9.2), myoglobin (horse, $M_r = 17$ kDa, pI 7.2), and hemoglobin (human, $M_r = 65$ kDa, pI 7.2) were from Sigma Chemical (St. Louis, MO). Molecular masses were confirmed by mass spectrometry. All three proteins contain heme groups and are reddish-brown. Cytochrome c solutions were prepared in phosphate buffer at pH 6.5, myoglobin in acetate buffer at pH 5.0, and hemoglobin in both phosphate (pH 6.5) and acetate (pH 5.0) buffers. All buffers contained 20 mM Na and were prepared from the sodium salts of each buffer with the pH adjusted with either phosphoric acid or acetic acid.

Preparation and characterization of SP-agarose matrix

Agarose (6% w/v) was dissolved in distilled, deionized water at 95°C. The solution was then used to prepare spheres for macroscopic studies or thin slabs cast into microfluidics chips for microscopic observations using the following procedures.

Agarose spheres were prepared by emulsifying the agarose solution in cyclohexane containing 2% (w/v) SPAN 85. The cyclohexane was first heated to 60°C in a 1,000 cm^3 baffled vessel placed in a thermostatted water bath (Brinkmann MGW Lauda RCS, RC20) and stirred at 1,000 rpm with a 5 cm diameter marine propeller. The agarose solution was then added drop-wise to a final ratio of 1 volume of agarose per 20 volumes of cyclohexane. After stirring for 10 min, the suspension was cooled by rapidly adding ice to the water bath reaching 25°C in 5 min. The agarose spheres formed were collected, washed first with 20% ethanol and then with water, and sieved through a 250 μm mesh screen to remove very large agarose particles and any aggregates.

SP-agarose particles were prepared from the neutral agarose particles obtained in this manner with the following procedure.[24] The particles were first crosslinked by reaction with a mixture containing 1.0 cm^3 of 1 N NaOH, 0.46 cm^3 of water, and 0.23 cm^3 of epichlorohydrin per cm^3 of settled particles for 3 h at room temperature on an orbital shaker. Next, the crosslinked particles were allylated by reaction with a solution containing 1 cm^3 of 1 N NaOH, 0.004 g of sodium borohydride, 0.13 g of Na_2SO_4, 0.4 cm^3 of water, and 0.46 cm^3 of AGE per cm^3 of settled particles for 13 h at 45°C. Finally, the allylated particles were sulfonated by reaction with a mixture containing 0.18 g of $Na_2S_2O_5$ and 51 cm^3 of water/cm^3 of settled particles. For the last step, following addition of the reactants, the solution was titrated to pH 6.5 with 50% NaOH and the reaction allowed to proceed for 12 h at 25°C. Following each step the matrix was washed with a large volume of water. The chemical steps used to functionalize the agarose slabs (see description below) were exactly the same.

The particle-size distribution (PSD) of the SP-agarose matrix was obtained from microphotographs at 100× magnification and varied somewhat from run to run. Three samples with average particles diameters of 64, 79, and 87 μm were used in this study. The corresponding PSD's are shown in Figure 2.

The charge density was determined by titration. For this purpose, a sample of the SP-agarose particles (~5 cm^3) was suspended in 100 cm^3 of 1 M HCl and mixed for 1.5 h. The particles were then separated from the supernatant and washed with distilled water in a Büchner funnel until the filtrate reached pH 7.0. The particles were then quantitatively transferred to a beaker with 50 cm^3 of a solution containing 0.04 M NaOH and 0.5 M NaCl and allowed to equilibrate for 2 h under gentle agitation. An aliquot of the supernatant was back titrated with standardized 0.1 M HCl. The charge density, determined from the amount of hydroxide consumed in the process, was found to be 150 ± 5 μmol/cm^3 of particle.

The effective pore size was determined by iSEC with dextran probes (5, 10, 25, 40, 70, and 500 kDa) and glucose. These experiments were done with the particles flow packed in 0.5 × 10 cm Tricorn columns (GE Healthcare, Piscataway, NJ) at 300 cm/h with a Waters HPLC system using a refractive index detector (Waters, Model R401). The mobile phase was 10 mM Na_2HPO_4 at a flowrate of 0.25 cm^3/min (76 cm/

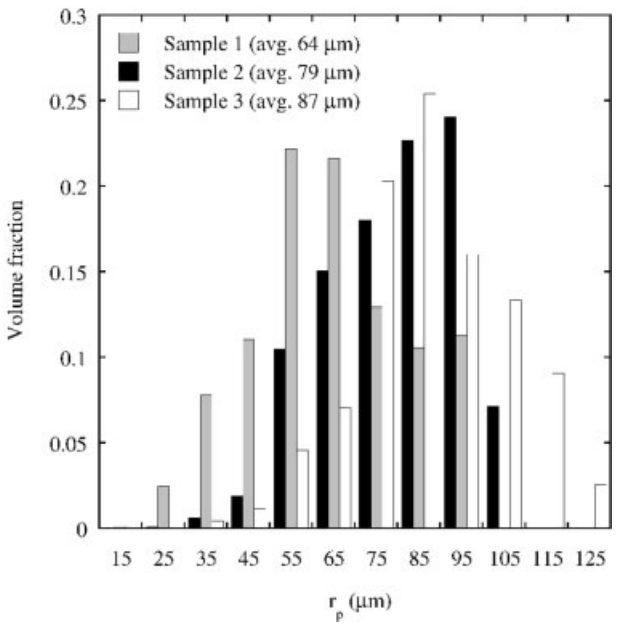

Figure 2. Particle-size distribution of SP-agarose samples.

h) with 0.02 cm^3 injections of 5 mg/cm^3 samples of the dextran and glucose standards. The distribution coefficient, K_d, was calculated from the apical retention volume, V_r, according to

$$K_d = \frac{V_r - V_0}{V_t - V_0} \quad (1)$$

where V_0 is the extraparticle or excluded volume and V_t is the total mobile phase volume. Blue dextran and glucose were used to determine V_0 and V_t, respectively. The apparent pore size was determined by regression from log K_d vs log R_η curves assuming a single cylindrical pore model.[25,26] Accordingly,

$$K_d = \left(1 - \frac{r_s}{r_{pore}}\right)^2 \quad (2)$$

where r_s is the radius of the solute and r_{pore} is the apparent pore radius. The former was taken equal to R_η −0.4 nm, where 0.4 nm is the radius of glucose and R_η is the viscosity radius calculated from the equation[25]

$$R_\eta = 0.0271(M_p)^{0.498} \quad (3)$$

where M_p is the dextran peak molecular mass.

Protein adsorption isotherms were obtained by equilibrating small samples of the SP-agarose spheres with protein solutions of known initial concentration in test tubes rotated end-to-end at 30 rpm. The amount of protein adsorbed was determined by material balance using the UV absorbance of the supernatant after 8 h, which was determined to be sufficient to attain equilibrium.

Transient batch protein uptake curves were obtained using a stirred vessel.[4] Briefly, samples of the SP-agarose particles (0.1–0.4 cm^3) were added to 60 cm^3 of the protein solution and stirred with a magnetically driven Teflon impeller at 300 rpm. The bulk protein concentration was continuously measured by rapidly circulating a stream of the supernatant through a Model UV-1 spectrophotometric detector from GE Healthcare (Piscataway, NJ) at 280 nm. The adsorbed concentration was obtained by mass balance at each time. The amount of particles added in each experiment was chosen to give approximately a 50% change in the bulk protein concentration to ensure precision in the measurements.

Microscopic experiments

To visualize the protein concentration profiles during transient adsorption and desorption, thin agarose slabs were prepared by casting the hot agarose solution in preheated microfluidics chips using the following procedure. The chips were prepared by etching Borofloat® glass slides with HF to a depth of 100 μm with the pattern shown in Figure 3. The pattern comprises a 5 mm wide flow channel with a 5 mm long side pocket for casting the gel. Side arms were incorporated in the pocket design to help physically anchor the gel and to prevent it from moving during the subsequent functionalization steps. The design also includes four 100 μm deep wells, which were filled with standard protein solutions (25–175 mg/cm^3) for calibration purposes to convert the color intensity to protein concentration.

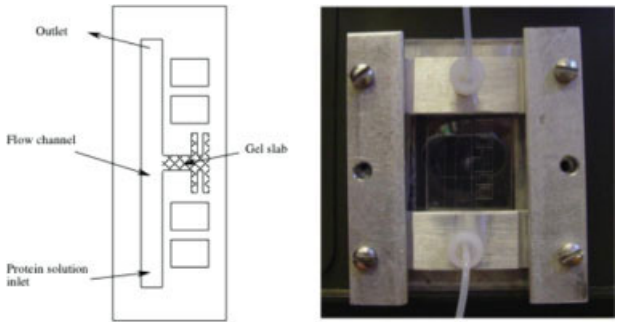

Figure 3. Etched pattern and microfluidics device for imaging protein concentration profiles.

The small rectangles are wells containing protein solutions for calibration purposes. [Color figure can be viewed in the online issue, which is available at www.interscience.wiley.com]

In order to cast the gel, the side pocket was covered with a small piece of Borofloat® glass held together with a metal clamp. The assembly was then pre-heated to 95°C, and the pocket filled by capillary action with the agarose solution dispensed by a small dropper. After allowing the gel to set at room temperature, the glass cover was removed to functionalize the agarose as described previously. During this process, the gel slab was held in place by a nylon mesh clamped in a Teflon holder. After functionalization, a glass slide with two holes drilled at positions corresponding with the flow channel was used to seal the assembly, which was held together by an aluminum frame as seen in Figure 3.

Adsorption experiments were performed by pumping a protein solution through the flow channel and across the exposed edge of the gel using a Model 22 syringe pump from Harvard Apparatus (Holliston, MA) at a flow rate of 1 cm^3/h, corresponding to an average velocity of 200 cm/h. Desorption experiments were done in a similar manner by pumping a buffer containing 500 mM NaCl and no protein. In either case, the protein concentration profiles in the gel were observed at 100× magnification with a Nikon Eclipse E200 microscope, imaged using a color CCD camera (Sanyo Hi-resolution, VCC-3972), and the images digitized using the public domain ImageJ software (developed at the U.S. National Institutes of Health and available on the Internet at http://rsb.info.nih.gov/ij/). Adsorbed protein concentration profiles were obtained from the gray-scale intensity of the digitized images smoothed using the Savitzky-Golay method with a weighted average of 5 points before and 5 points after each pixel. The relationship between gray-scale intensity and protein concentration was determined by filling the calibration wells with protein solutions of known concentration and was linear over the range of the experimental measurements.

Results and Discussion

Apparent pore size

As discussed in the Materials and Methods section, apparent pore size, protein adsorption isotherms, and protein adsorption kinetics were obtained from macroscopic experiments. Figure 4 show the iSEC peaks for the neutral agarose matrix and for the SP-functionalized material while Figure 5

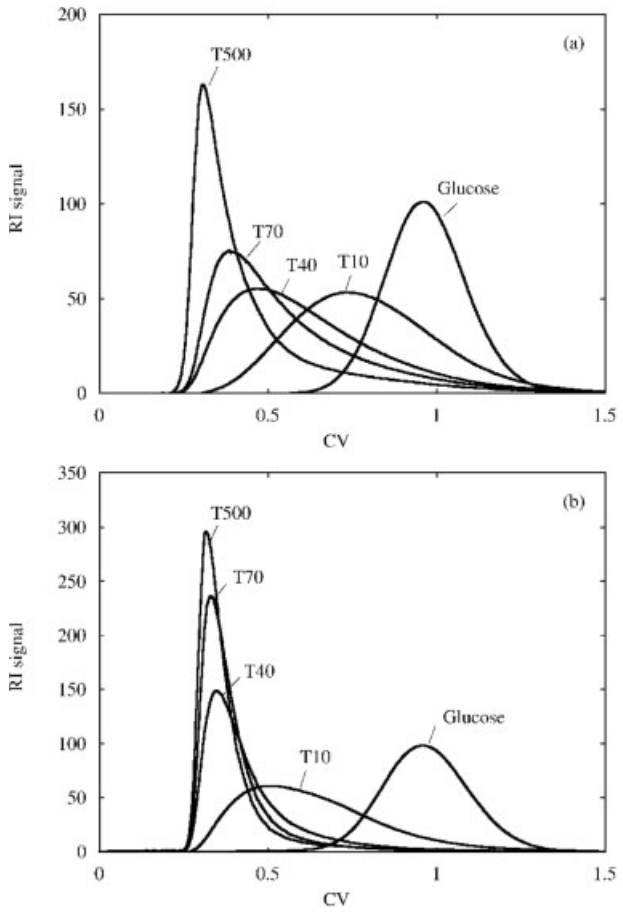

Figure 4. iSEC peaks for the agarose base matrix (a) and the SP-functionalized agarose particles (b) for sample 1.

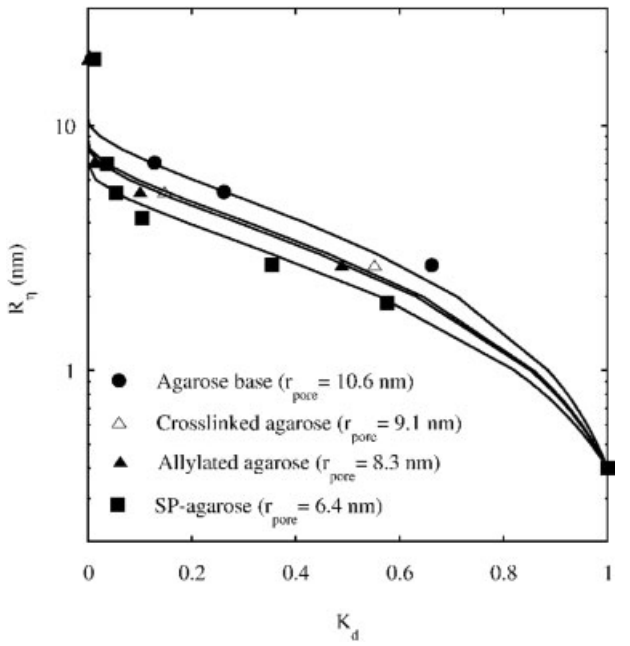

Figure 5. iSEC selectivity curves for agarose, crosslinked agarose, allylated agarose, and SP-agarose particles (sample 1).

Solid lines are calculated from Eq. 2 with the apparent pore radii in the figure legend.

shows the corresponding selectivity curves. As seen in Figure 4a, the dextran probes are all resolved with the agarose base matrix. However, only the 10 kDa dextran is resolved with the SP-agarose matrix with all the larger dextrans coeluting within the extraparticle volume (Figure 4b). The corresponding apparent pore radius, estimated from Eq. 2, is reduced from 10.6 nm for the base matrix to 6.4 nm for the SP-functionalized material. Figure 5 also shows the experimental K_d-values following the crosslinking and allylation steps, but prior to the introduction of the ionic groups. The corresponding apparent pore radii are intermediate (9.1 and 8.3 nm); however, it is evident that while crosslinking and allylation have some effects, introduction of the sulfonic acid groups is the main contribution to the decreased pore size.

Adsorption isotherms

Adsorption isotherms for cytochrome c, myoglobin, and hemoglobin are shown in Figure 6. The adsorption capacity is different for the different proteins and varies with pH, but the isotherms are very favorable in all cases. Adsorbed cytochrome c at pH 6.5 could be completely desorbed by exposing the protein-loaded particles to 500 mM NaCl. However, little desorption was obtained in 500 mM NaCl for myoglobin (19% desorbed) and for hemoglobin at pH 5.0 (15% desorbed) suggesting that adsorption of these two proteins is nearly irreversible for these conditions. Desorption of hemoglobin at pH 6.5 was nearly complete (95% desorbed) in 500 mM NaCl indicating weaker binding when the pH is closer to the protein's isoelectric point. The reasons why the pH 5 hemoglobin adsorption capacity is so much larger than

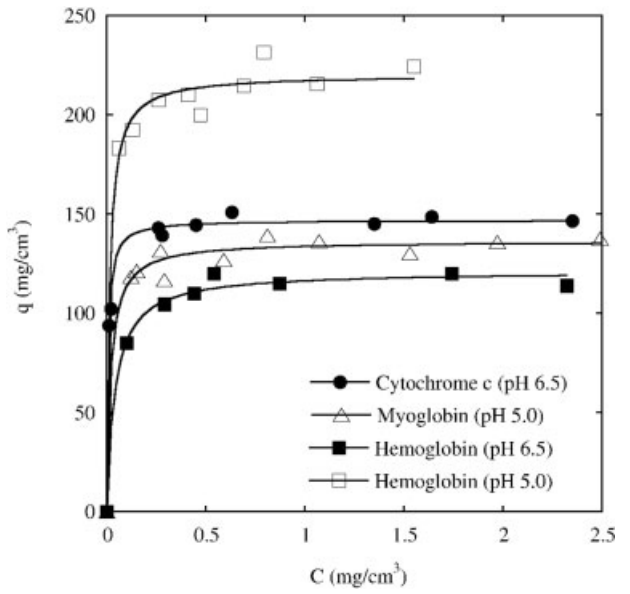

Figure 6. Adsorption isotherms for cytochrome c, myoglobin, and hemoglobin on SP-agarose particles.

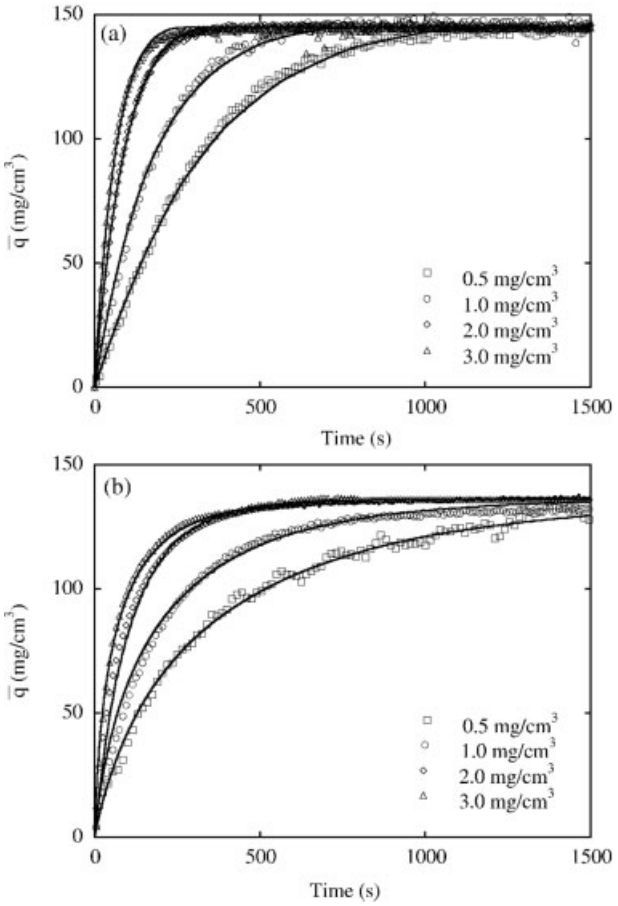

Figure 7. Batch uptake curves for cytochrome c (a) and myoglobin (b) obtained with different initial protein concentrations.

Solid lines are based on the effective pore diffusion model including the PSD[24] with the D_e-values in Table 1.

for cytochrome c or myoglobin at the same pH are not clear. One possibility is that hemoglobin could be adsorbed in two different configurations. Indeed, hemoglobin is not spherical[27] and might be adsorbed in a more favorable configuration when farther away from the pI. Another possibility is dissociation of the hemoglobin tetramer into its $\alpha\beta$ subunits, which is known to be dominant in dilute solutions at low pH but insignificant at pH 6.5.[28,29]

Batch adsorption kinetics

Figure 7 shows the batch uptake curves for cytochrome c and myoglobin with initial protein concentrations of 0.5, 1, 2, and 3 mg/cm^3. For both proteins there is a large dependence of the rate on concentration. However, in spite of the fact that the particles used for the cytochrome c experiments were somewhat larger, the uptake rate of cytochrome c is much faster than for myoglobin, especially at the lower concentrations. Figure 8 shows a comparison of the batch uptake curves for the different proteins, including hemoglobin at pH 5.0 and 6.5, with an initial protein concentration of 2 mg/cm^3. To facilitate the comparison, the data are presented in terms of the fractional approach to saturation $(\bar{q}/q_m)$ as a function of time normalized by the square of the average particle radius, $\bar{r}_p$. As seen in this figure, the rate of approach to saturation varies substantially from protein to protein and with pH suggesting that specific interactions of the protein with the adsorbent surface influence the mass transfer rate.

Microscopic experiments

Figures 9 and 10 show the images and digitized concentration profiles for the adsorption of cytochrome c and myoglobin in the SP-agarose matrix at protein concentrations of 3 and 0.5 mg/cm^3, respectively. The profiles are shown normalized by the equilibrium adsorption capacity q_m. These values are, however, nearly the same for these two proteins and practically independent of protein concentration (cf. Figure 6) so that the profiles can be compared directly. This comparison shows that not only the uptake rates are very different for the two proteins, but that the concentration profiles are also quantitatively and, especially, qualitatively different. Myoglobin results in much sharper profiles approximately consistent with a pore diffusion mechanism (cf. Figure 1), while cytochrome c results in smoother, diffuse profiles. The effect of the fluid phase protein concentration is also dramatically different for the two proteins. As seen in Figure 10, at 0.5 mg/cm^3 the protein concentration at the exposed edge of the gel approaches equilibrium very slowly in the case of cytochrome c (Figure 10a), but comparatively quickly in the case of myoglobin (Figure 10b). In addition, the profiles are very diffuse for cytochrome c, but remain sharp for myoglobin. This behavior suggests that a transport or kinetic resistance at the fluid-gel interface has a substantial effect, possi-

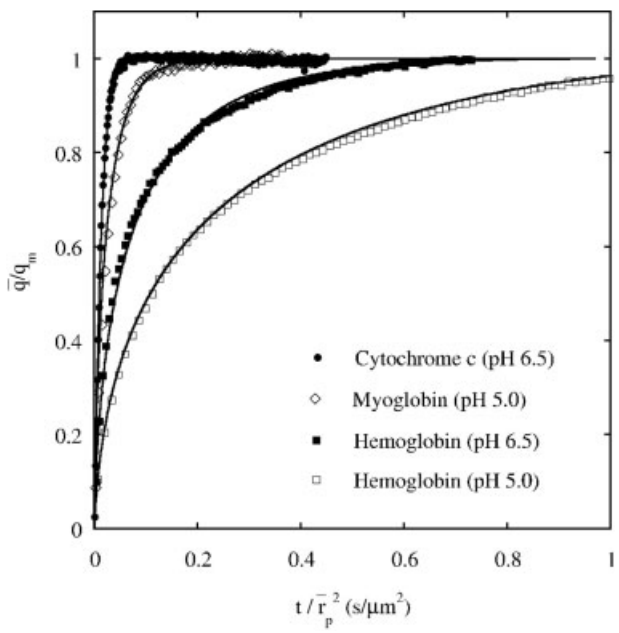

Figure 8. Batch uptake curves plotted vs. the normalized time $t/\bar{r}_p^{-2}$ for cytochrome c, myoglobin, and hemoglobin with C_0 = 2 mg/cm^3.

Solid lines are based on the effective pore diffusion model including the PSD[24] with the D_e-values in Table 1.

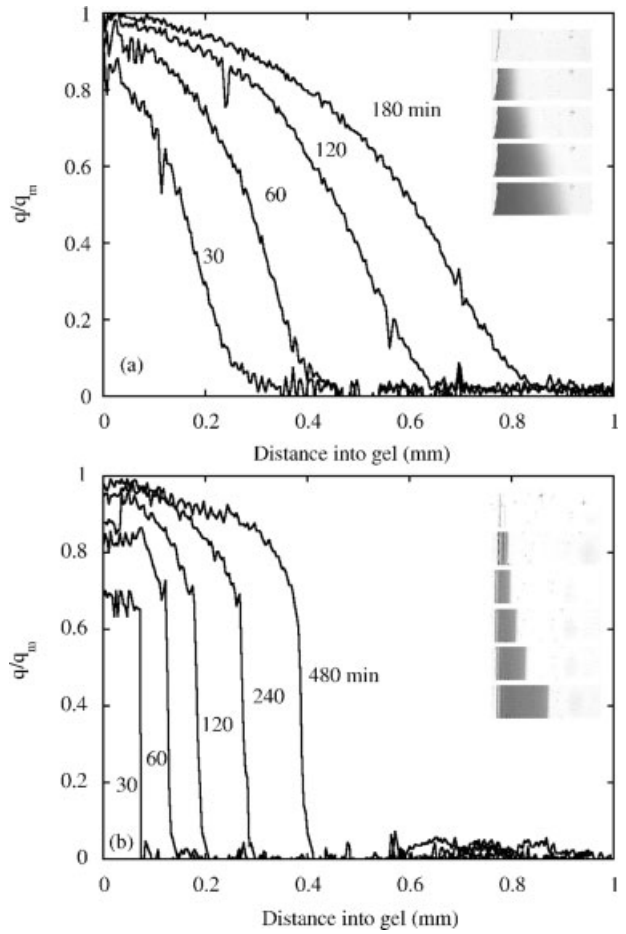

Figure 9. Gray-scale images and digitized concentration profiles for protein adsorption in SP-agarose slabs with C = 3 mg/cm^3 for cytochrome c at pH 6.5 (a) and myoglobin at pH 5.0 (b).

bly limiting the rate of adsorption of cytochrome c at this lower concentration.

Figures 11a and b show the hemoglobin concentration profiles for a 2 mg/cm^3 protein concentration and at pH 5.0 and 6.5, respectively. The profiles are again normalized by the equilibrium value q_m, which, in this case, is very different at the two different pH values. Thus, only the shapes of the profiles can be compared directly. At pH 5.0 (Figure 11a), the profiles are sharper and advance more slowly in the gel, while at pH 6.5 they are rather diffuse and progress more quickly. These differences can be ascribed in part to the higher adsorption capacity at pH 5.0. However, even at pH 6.5, the adsorption isotherm of hemoglobin is quite favorable (cf. Figure 6), which would result in sharp profiles if pore diffusion were the controlling mechanism. The much smoother profiles obtained experimentally suggest again that a more complex mechanism is responsible for protein transport at this pH. The relationship between the radius of hemoglobin in its tetrameric form (~2.5 nm based on its diffusion coeffcient) and the apparent pore radius as determined by iSEC (~6.4 nm) provides further insight. For these conditions, pore diffusion of the hemoglobin tetramer would be expected to be highly hindered because of steric[30] and charge repulsion effects.[15] Nevertheless, the adsorption rates are relatively high indicating that factors other than ordinary pore diffusion contribute to protein transport. Dissociation of hemoglobin into its $\alpha\beta$ subunits could also be a factor. As noted by Guidotti and Craig,[29] hemoglobin exhibits much lower membrane rejection in dialysis membranes than expected from its size, especially at lower pH values, as a result of its dissociation into smaller units. A similar effect could explain the observed hemoglobin adsorption behavior, with the smaller subunits providing faster transport in the agarose pores. Of course, in our case the situation is more complex since both tetramer and dissociated forms also interact with the SP-groups.

Further insight is obtained by examining the desorption behavior. As previously noted, cytochrome c adsorbed on the SP-agarose particles was desorbed quantitatively with 500 mM NaCl, while little desorption was seen for myoglobin. The corresponding desorption behavior for these two proteins in the microfluidics chip can be seen in Figure 12. In these experiments, each protein was adsorbed for a given time (3 h for cytochrome c and 8 h for myoglobin), after which the gel was exposed to a 500 mM NaCl buffer containing no protein. For cytochrome c (Figure 12a), the protein concentration at the gel-fluid interface is almost instantly reduced to zero, and desorption is rapid and essentially complete in 120 min. Con-

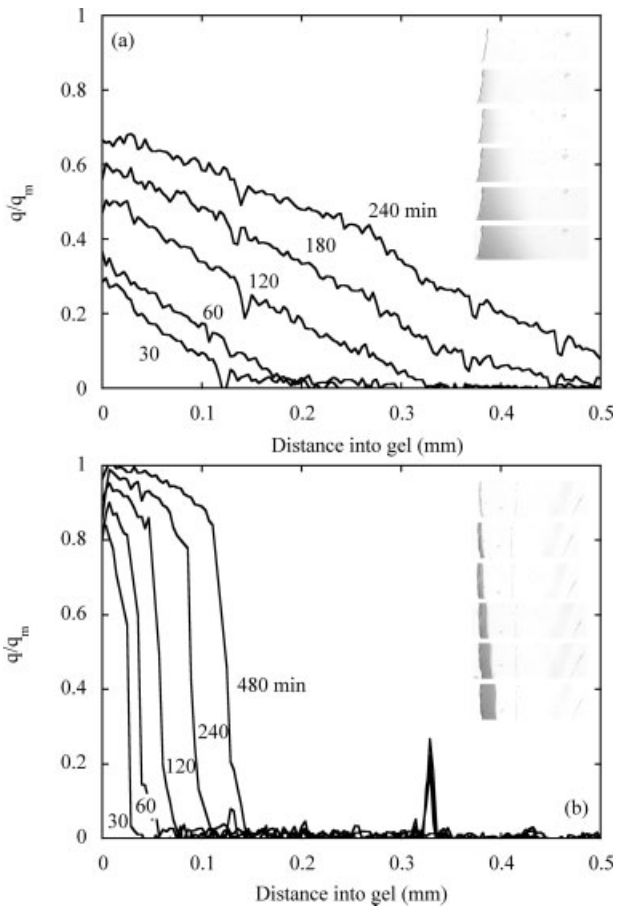

Figure 10. Same as Figure 9 but with C = 0.5 mg/cm^3 for cytochrome c (a) and myoglobin (b).

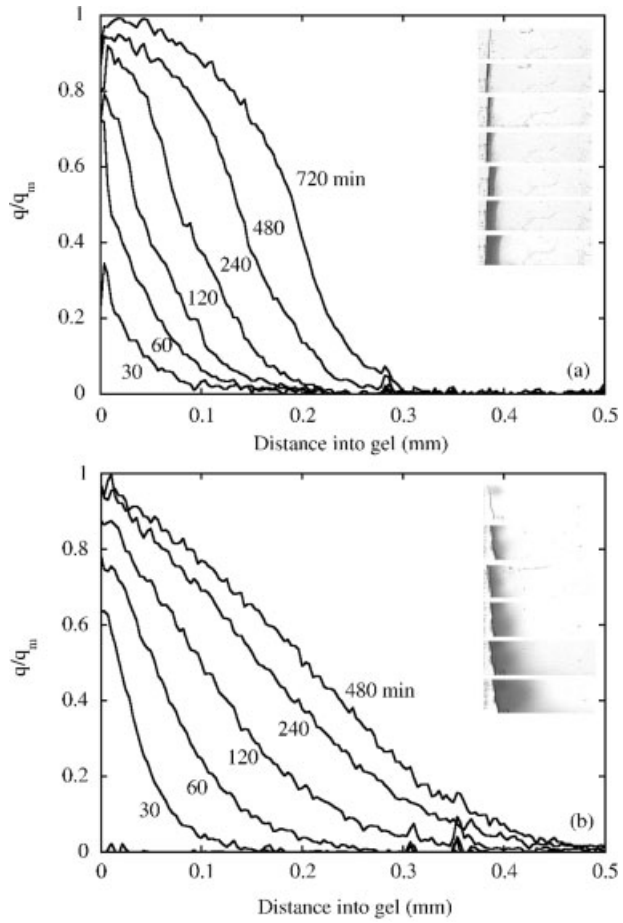

Figure 11. Gray-scale images and digitized concentration profiles for protein adsorption in SP-agarose slabs with C = 2.0 mg/cm^3 for hemoglobin at pH 5.0 (a) and pH 6.5 (b).

versely, for myoglobin (Figure 12b), the concentration profile changes very little after exposure to 500 mM NaCl, suggesting that the bulk of this protein is very tightly bound to the SP-agarose matrix. Some desorption appears to occur near the interface indicating that a small percentage of this protein might be more weakly bound in a different state or configuration.

Mass transfer modeling

The development of a detailed mechanistic model capable of describing the experimental data is beyond the scope of this work. Nonetheless, it is useful to summarize the results in terms of a simple, mass transfer limited kinetic model where protein transport in the SP-agarose matrix is assumed to occur via a pore diffusion mechanism. In this case, an effective pore diffusion coefficient, D_e, lumping together all transport mechanisms is used as a fitted parameter. While such an approach is simplistic and is likely to result in D_e-values which vary with concentration, it permits a comparison of adsorption kinetics measurements obtained from macroscopic and microscopic experiments since, as a minimum, the effects of the different time and length scales should be described correctly.[3] Moreover, since D_e is expected to be less than the free solution diffusivity and essentially independent of protein concentration for a pore diffusion mechanism, its magnitude can provide information about any possible enhancement of the transport mechanism as a result of either interactions between the protein and the adsorbent surface (e.g. surface diffusion) or electrokinetic effects.[12–13,31]

The model used here to describe the batch uptake data assumes a rectangular isotherm and considers explicitly the experimental particle-size distribution as discussed by Carta and Ubiera.[32] The model equations, including the effect of the external mass transfer resistance can be found in Stone and Carta.[24] The film mass transfer coefficient was estimated with the correlation of Armenante and Kirwan.[33] The fitted D_e-values, normalized by the free solution diffusivity, D, are summarized in Table 1 and calculated curves are shown by the solid lines in Figures 7 and 8. The D-values were obtained from Tyn and Gusek[34] and were 1.2×10^{-6}, 1.1×10^{-6}, and 0.63×10^{-6} cm^2/s for cytochrome c, myoglobin, and hemoglobin, respectively. As seen in Table 1, the D_e/D-values for cytochrome c are much larger than unity and increase as the protein concentration is decreased. Conversely, for myoglobin (Figure 12b), the concentration profile changes very little after exposure to 500 mM NaCl, suggesting that the bulk of this protein is very tightly bound to the SP-agarose matrix. Some desorption appears to occur near the interface indicating that a small percentage of this protein might be more weakly bound in a different state or configuration.

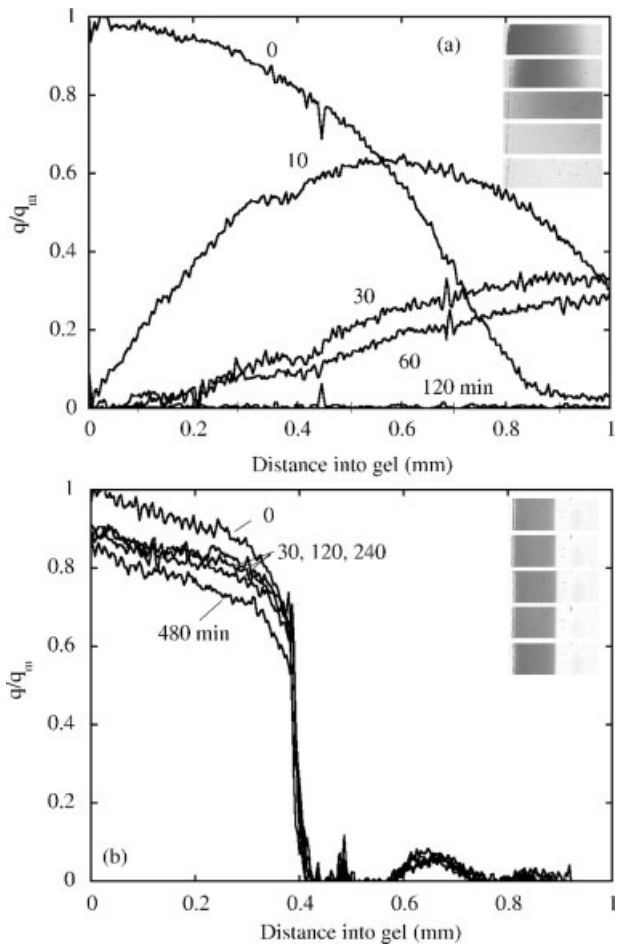

Figure 12. Gray-scale images and digitized concentration profiles for protein desorption from SP-agarose slabs using 500 mM NaCl.

(a) Cytochrome c adsorbed for 180 min and (b) myoglobin adsorbed for 480 min, each from a 3 mg/cm^3 solution.

Table 1. Values Determined from Batch Adsorption Experiments

C_0 (mg/cm^3)	3.0	2.0	1.0	0.5
Cytochrome c* (pH 6.5)	5.7	9.8	16.2	32.5
Myoglobin† (pH 5.0)	1.8	1.5	1.8	2.2
Hemoglobin‡ (pH 6.5)	nd	0.79	nd	nd
Hemoglobin§ (pH 5.0)	nd	0.43	0.63	nd

*$\bar{r}_p = 79$ μm, $k_f = 1.9 \times 10^{-3}$ cm/s, $D = 1.2 \times 10^{-6}$ cm^2/s.
$^{\dagger}\bar{r}_p = 64$ μm, $k_f = 2.1 \times 10^{-3}$ cm/s, $D = 1.1 \times 10^{-6}$ cm^2/s.
$^{\ddagger}\bar{r}_p = 64$ μm, $k_f = 1.9 \times 10^{-3}$ cm/s, $D = 0.63 \times 10^{-6}$ cm^2/s.
$^{\S}\bar{r}_p = 87$ μm, $k_f = 0.87 \times 10^{-3}$ cm/s, $D = 0.63 \times 10^{-6}$ cm^2/s.

versely, for myoglobin these values are around 1 and vary only slightly with protein concentration. Lower values are obtained for hemoglobin, with the D_e/D-values at pH 5.0 and 6.5 being surprisingly similar despite the obviously qualitative differences in the experimental concentration profiles at the two different pH values. Clearly, although the model fits appear to be satisfactory, they offer only limited insight into the nature of the mass transfer mechanism.

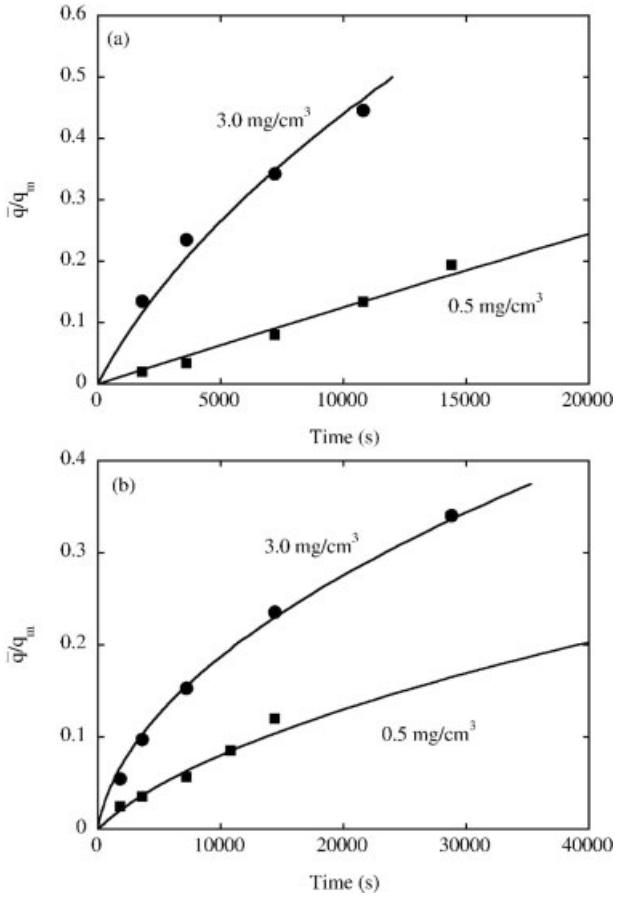

Figure 13. Uptake curves for SP-agarose slabs determined by averaging the profiles over a 0.1 cm length for cytochrome c (a) and myoglobin (b).

Solid lines are based on the effective pore diffusion model with D_e values in Table 2.

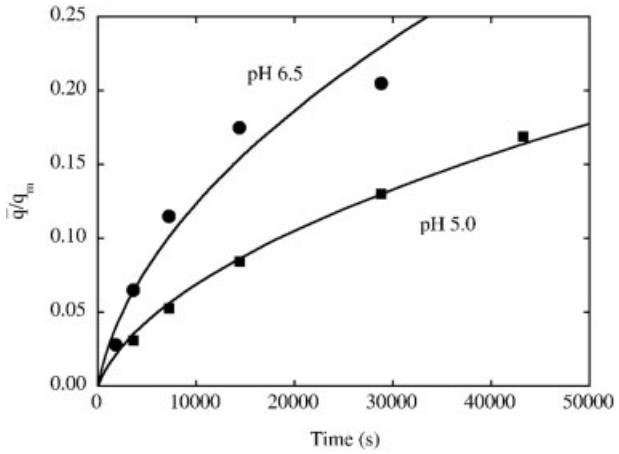

Figure 14. Same as Fig. 12 but for 2 mg/cm^3 hemoglobin at pH 6.5 and 5.0.

Solid lines are based on the effective pore diffusion model with D_e values in Table 2.

The same assumptions made for modeling the batch uptake curves were made for the analysis of the microscopic data. The following equation is obtained for pore diffusion with a rectangular isotherm for the rectilinear geometry of the SP-agarose slab experiments:[35]

$$\frac{tD_e}{l^2}\ \frac{C}{q_m} = \frac{1}{2}\left(\frac{\bar{q}}{q_m}\right)^2 + \frac{1}{Bi}\left(\frac{\bar{q}}{q_m}\right) \tag{4}$$

where C is the protein concentration in the bulk liquid, $\bar{q}$ is the average protein concentration in the slab, l its length, and $Bi = k_f l/D_e$ is the Biot number. In analogy to the batch adsorption experiments, the effective pore diffusivity D_e can be thus found by fitting Eq. 4 to the $\bar{q}$ vs t uptake curves, where $\bar{q}$ is obtained from the digitized concentration profiles at each time. These curves are shown in Figures 13 and 14. Since, in practice, the concentration profiles did not extend beyond a 0.1 cm distance from the interface, we based the calculation of $\bar{q}$ on $l = 0.1$ cm.

The film mass transfer coefficient, k_f, for the microscopic adsorption experiments was estimated as follows. On the basis of the batch uptake data, the D_e-value for cytochrome c is expected to be on the order of 4×10^{-5} cm^2/s at 0.5 mg/cm^3 (cf. Table 1). The Sherwood number ($Sh = k_f d/D$) for the geometry of our device is not known precisely. However, for laminar flow in rectangular ducts, Sh is expected to vary between 2.89 for square channels and 8.24 for flow between

Table 2. Values Determined from Microscopic Imaging Experiments

C (mg/cm^3)	3.0	2.0	0.5
Cytochrome c* (pH 6.5)	9.2	nd	external control
Myoglobin† (pH 5.0)	0.91	nd	2.0
Hemoglobin‡ (pH 6.5)	nd	0.95	nd
Hemoglobin‡ (pH 5.0)	nd	0.63	nd

*$k_f = 3.7 \times 10^{-4}$ cm/s, $D = 1.2 \times 10^{-6}$ cm^2/s.
$^{\dagger}k_f = 3.4 \times 10^{-4}$ cm/s, $D = 1.1 \times 10^{-6}$ cm^2/s.
$^{\ddagger}k_f = 1.7 \times 10^{-4}$ cm/s, $D = 0.63 \times 10^{-6}$ cm^2/s.

parallel plates.[36] In turn, assuming that the characteristic length for transport in the fluid phase, d, is the depth of the flow channel (100 μm), the Biot number, $Bi = \frac{D}{D_e}\frac{l}{d}Sh$, is expected to be between 0.8 and 2. Such small values indicate that the film mass transfer resistance is likely to be controlling for these conditions, especially for relatively short times. In this case, Eq. 4 reduces to:

$$\frac{\bar{q}}{q_m} = \frac{C}{q_m}\frac{k_f t}{l} \tag{5}$$

indicating a linear relationship between average concentration in the slab and time. As seen in Figure 13a, this linear relationship is indeed observed for the 0.5 mg/cm^3 cytochrome c data ($R^2 = 0.961$). Accordingly, by regression, we obtain $k_f = 3.7 \times 10^{-4}$ cm/s, which corresponds to Sh ~3.4, close to the expected limiting value. Since k_f should depend only on hydrodynamic conditions, we estimated the film mass transfer coefficient for the other two proteins by assuming that Sh is the same.

Table 2 summarizes the fitted D_e-values and Figures 13 and 14 show the calculated curves in comparison with the data. The D_e-values are similar to the macroscopically derived ones indicating that the two different types of measurements are consistent. Quantitative differences between the values exist. However, they can be ascribed to the fact that the simple pore diffusion model used is clearly inadequate for the cases where the concentration profiles are not sharp and fail to provide a physically correct representation of the mass transfer mechanism. This is especially true for cytochrome c (where the concentration profiles are rather diffuse) and for hemoglobin (where dissociation may play a role) whose profiles deviate substantially from the model's underlying assumption. More sophisticated models, accounting explicitly for protein-surface and possibly protein-protein interactions are apparently needed to correctly predict the protein adsorption kinetics.

Conclusions

This study has focused on the development of a method to visualize protein adsorption and transport in charged agarose gels on a microscopic scale and on a quantitative comparison of the results with those obtained from conventional macroscopic batch uptake measurements. The method does not require protein labeling and uses gels cast in a slab-shape allowing study of transport in a rectilinear, essentially semi-infinite geometry. Microscopic and macroscopic measurements are found to be consistent for several proteins studied and both data sets can be described using an effective pore diffusion model. On the other hand, the microscopic measurements of protein concentration profiles reveal that despite the observed qualitative agreement with this model, the adsorption kinetics depends on a more complex transport mechanism. Specific protein-surface interactions obviously affect the rate of adsorption. In particular, the binding strength and its reversibility in response to increasing the ionic strength appear to play a dominant role. For example, fast rates of adsorption and diffuse concentration profiles were observed for cytochrome c, which, in spite of exhibiting a very favorable isotherm at low ionic strength, was completely desorbed in 500 mM NaCl. Conversely, much lower rates and sharp concentration profiles were observed for myoglobin and hemoglobin at pH 5, conditions where both proteins appeared to be adsorbed nearly irreversibly with little desorption (19 and 15%, respectively) in 500 mM NaCl. Hemoglobin at pH 6.5 appears to be an intermediate case exhibiting nearly complete desorption (95%) in 500 mM NaCl and diffuse concentration profiles, but relatively slow adsorption kinetics.

At this point, the mechanistic reasons for these varying behaviors are not precisely known. One possibility is transport in the adsorbed phase. While the diffuse profiles observed are obviously more complex than could be predicted by a simple adsorbed phase diffusion model with constant diffusivity (cf. Figure 1), the results suggest that this transport mechanism may explain rapid protein adsorption kinetics in these materials. The agarose matrix used in these studies has a rather small pore size, which might result in overlapping electrical double layers. Provided the protein retains mobility, rapid transport could occur in these pores because of the high concentration driving force.[37–39] Such a mechanism could not, of course, be a factor for proteins that retain little diffusional mobility because they are either irreversibly bound or too large to fit in the pores. Electrokinetic effects could also play a role if protein transport is thermodynamically coupled to an electrochemical potential gradient.[12,40] These coupled transport effects have been also shown, theoretically, to potentially lead to overshoots in the protein concentration profile, with the adsorbed protein temporarily exceeding the final equilibrium value. Such overshoots were not seen in our experimental observations although it should be noted that we studied different proteins and different conditions from those for which overshoots have been predicted.[12,40] In either case, the new method and measurements described herein should provide an effective way of testing hypotheses regarding the mechanisms that affect protein transport in these charged gels.

Notation

Bi = Biot number
C = concentration in the fluid phase, mg/cm^3
C_0 = initial concentration in the fluid phase, mg/cm^3
CV = number of column volumes
d = depth of flow channel, cm
D = free solution diffusivity, cm^2/s
D_e = effective pore diffusivity, cm^2/s
D_s = adsorbed phase diffusivity, cm^2/s;
K_d = distribution coefficient;
k_f = external film mass transfer coefficient, cm/s
l = length of slab, mm
M_p = peak molecular mass, kDa
M_r = protein molecular mass, kDa
q = protein concentration in gel, mg/cm^3
$\bar{q}$ = average protein concentration in gel, mg/cm^3
q_m = adsorption capacity, mg/cm^3
r_p = particle radius, cm
$\bar{r}_p$ = average particle radius, cm
r_{pore} = apparent pore radius, nm
r_s = solute radius, nm
R_η = viscosity radius, nm
Sh = Sherwood number
t = time, s
V = volume of liquid, cm^3
V_0 = extraparticle volume, cm^3

V_r = peak retention volume, cm^3
V_t = total mobile phase volume, cm^3

Acknowledgments

The work was supported by NSF Grant No. CTS-0414143 and the ARCS Foundation. The authors are grateful to the microfabrication laboratory of Prof. James Landers at the University of Virginia for their help with the fabrication of the microfluidics chips.

Literature Cited

1. Guiochon G, Felinger A, Shirazi DG, Katti AM. Fundamentals of Preparative and Nonlinear Chromatography, 2nd edition. New York: Elsevier Academic Press, 2006.
2. Jansen JC, Rydén L.Protein Purification—Principles, High Resolution Methods and Applications. New York:VCH, 1989.
3. LeVan MD, Carta G, Yon CM.Adsorption and Ion Exchange. In: Perry RH, Green DW.Perry's Chemical Engineers' Handbook, 7th edition. New York: McGraw-Hill, 1997. (Section 16).
4. Carta G, Ubiera AR, Pabst TM. Protein mass transfer kinetics in ion exchange media: Measurements and interpretations. *Chem Eng Tech* 2005;28:1252–1264.
5. Weaver LE, Carta G. Protein adsorption on cation exchangers: comparison of macroporous and gel-composite media. *Biotechnol Progr.* 1996;12:342–355.
6. Chang C, Lenhoff AM. Comparison of protein adsorption isotherms and uptake rates in preparative cation-exchange materials. *J Chromatogr A.* 1998;827:281–293.
7. Chen WD, Dong XY, Sun Y. Analysis of diffusion models for protein adsorption to porous anion-exchange adsorbent. *J Chromatogr A.* 2002;962:29–40.
8. Ljunglöf A, Hjorth R. Confocal microscopy as a tool for studying protein adsorption to chromatographic matrices. *J Chromatogr A.* 1996;743:75–83.
9. Linden T, Ljunglöf A, Hagel L, Kula MR, Thömmes J. Visualizing patterns of protein uptake to porous media using confocal scanning laser microscopy. *Sep Sci Tech.* 2002;37:1–32.
10. Hubbuch J, Linden T, Knieps E, Thömmes J, Kula MR. Dynamics of protein uptake within the adsorbent particle during packed bed chromatography. *Biotechnol Bioeng.* 2002;80:359–368.
11. Hubbuch J, Linden T, Knieps E, Ljunglöf A, Thöömmes J, Kula MR. Mechanism and kinetics of protein transport in chromatographic media studied by confocal laser scanning microscopy. I. The interplay of sorbent structure and fluid phase conditions. *J Chromatogr A.* 2003;1021:93–104.
12. Dziennik SR, Belcher EB, Barker GA, DeBergalis MJ, Fernandez SE, Lenhoff AM. From the cover: nondiffusive mechanisms enhance protein uptake rates in ion exchange particles. *Proc Nat Acad Sci.* 2003;100:420–425.
13. Dziennik SR, Belcher EB, Barker GA, Lenhoff AM. Effects of ionic strength on lysozyme uptake rates in cation exchangers. I. Uptake in SP Sepharose FF. *Biotechnol Bioeng.* 2005;91:139–153.
14. Ljunglöf A, Lacki KM, Mueller J, Harinnarayan C, van reis R, Fahrner R, Van Alstine JM. Ion exchange chromatography of antibody fragments. *Biotechnol Bioeng.* 2006;96:515–524.
15. Harinarayan C, Mueller J, Ljunglöf A, Farhner R, Van Alstine J, van Reis R. An exclusion mechanism in ion exchange chromatography. *Biotechnol Bioeng.* 2006;95:775–787.
16. Teske CA, Schroeder M, Simon R, Hubbuch J. Protein-labeling effects in confocal laser scanning microscopy. *J Phys Chem B.* 2005;109:13811–13817.
17. Teske CA, von Lieres E, Schroder M, Ladiwala A, Cramer SM, Hubbuch JJ. Competitive adsorption of labeled and native protein in confocal laser scanning microscopy. *Biotechnol Bioeng.* 2006;95:58–66.
18. Dziennik, SR.Ph.D Dissertation, Department of Chemical Engineering, University of Delaware, Newark, DE, 2002.
19. Lewus RK, Carta G. Protein diffusion in charged polyacrylamide gels: visualization and analysis. *J Chromatogr A.* 1999;865:155–168.
20. Lewus RK, Carta G. Protein transport in constrained anionic hydrogels: diffusion and boundary-layer mass transfer. *Ind Eng Chem Res.* 2001;40:1548–1558.
21. Russell SM, Belcher EB, Carta G. Protein partitioning and transport in supported cationic acrylamide-based hydrogels. *AIChE J.* 2003; 49:1168–1177.
22. Johnson EM, Deen WM. Hydraulic permeability of agarose gels. *AIChE J.* 1996;42:1220–1224.
23. Jin LJ, Giordano BC, Landers JP. Dynamic labeling during capillary or microchip electrophoresis for laser-induced fluorescence detection of protein-SDS complexes without pre- or postcolumn labeling. *Anal Chem.* 2001;73:4994–4999.
24. Stone MC, Carta G. Protein adsorption and transport in agarose and dextran-grafted agarose media for ion exchange chromatography. *J Chromatogr A.* 2007;1146:202–215.
25. Hagel L, Ostberg M, Andersson T. Apparent pore size distributions of chromatography media. *J Chromatogr A.* 1996;743:33–42.
26. DePhillips P, Lenhoff AM. Pore size distributions of cation-exchange adsorbents determined by inverse size-exclusion chromatography. *J Chromatogr A.* 2000;883:39–54.
27. Berman HM, Westbrook J, Feng Z, Gilliland G, Bhat TN, Wessig H, Shingyalov IN, Bourne PE. The Protein Data Bank. *Nucleic Acids Res.* 2000;235–242. (Available at http://www.pdb.org/).
28. Field EO, O'Brien JRP. Dissociation of human haemoglobin at low pH. *Biochem J* 1955;60:656–661.
29. Guidotti G, Craig LC. Dialysis studies, VIII. The behavior of solutes which associate. *Proc Nat Acad Sci USA.* 1963;50:46–54.
30. Deen WM, Hindered transport of large molecules in liquid-filled pores. *AIChE J.* 1987;33:1409–1425.
31. Yoshida H, Yoshikawa M, Kataoka T. Parallel transport of BSA by surface and pore diffusion in strongly basic chitosan. *AIChE J.* 1994;40:2034–2044.
32. Carta G, Ubiera A. Particle-size distribution effects in batch adsorption. *AIChE J.* 2003;49:3066–3073.
33. Armenante PM, Kirwan DJ. Mass-transfer to microparticles in agitated systems. *Chem Eng Sci.* 1989;44:2781–2796.
34. Tyn MY, Gusek, TW. Prediction of diffusion-coefficients of proteins. *Biotechnol Bioeng.* 1990;35:327–338.
35. Do DD. Adsorption Analysis: Equilibria and Kinetics. London: Imperial College Press, 1998.
36. Knudsen JG, Hottel HC, Sarofm AF, Wankat PC, Knaebel KS.Heat and mass transfer. In: Perry RH, Green DW, editors. Perry's Chemical Engineers' Handbook 7th edition. New York: McGraw-Hill, 1997:5–15(Section 5).
37. Fernandez MA, Carta G. Characterization of protein adsorption by composite silica-polyacrylamide gel anion exchangers. I. Equilibrium and mass transfer in agistated contactrs. *J Chromatogr A.* 1996;746: 169–183.
38. Hunter AK, Carta G. Protein adsorption on novel acrylamido-based polymeric ion-exchangers. II. Adsorption rates and column behavior. *J Chromatogr A.* 2000;897:81–97.
39. Farnan D, Frey DD, Horvath C. Surface and pore diffusion in macroporous and gel-filled gigaporous stationary phases for protein chromatography. *J Chromatogr A.* 2002;959:65–73.
40. Liapis AI, Grimes BA, Lacki K, Neretnieks I. Modeling and analysis of the dynamic behavior of mechanisms that result in the development of inner radial humps in the concentration of a single adsorbate in the adsorbed phase of porous adsorbent particles observed in confocal scanning laser microscopy experiments: diffusional mass transfer and adsorption in the presence of an electrical double layer. *J Chromatogr A.* 2001;921:135–145.

Manuscript received Dec. 27, 2006, and revision received Mar. 15, 2007.